Crystal Structures of the Anticancer Clinical Candidates R115777 (Tipifarnib) and BMS-214662 Complexed with Protein Farnesyltransferase Suggest a Mechanism of FTI Selectivity†

T. Scott Reid and Lorena S. Beese*

Department of Biochemistry, Duke University Medical Center, Durham, North Carolina 27710

Received February 6, 2004; Revised Manuscript Received March 26, 2004

ABSTRACT: The search for new cancer therapeutics has identified protein farnesyltransferase (FTase) as a promising drug target. This enzyme attaches isoprenoid lipids to signal transduction proteins involved in growth and differentiation. The two FTase inhibitors (FTIs), R115777 (tipifarnib/Zarnestra) and BMS-214662, have undergone evaluation as cancer therapeutics in phase I and II clinical trials. R115777 has been evaluated in phase III clinical trials and shows indications for the treatment of blood and breast malignancies. Here we present crystal structures of R115777 and BMS-214662 complexed with mammalian FTase. These structures illustrate the molecular mechanism of inhibition and selectivity toward FTase over the related enzyme, protein geranylgeranyltransferase type I (GGTase-I). These results, combined with previous biochemical and structural analyses, identify features of FTase that could be exploited to modulate inhibitor potency and specificity and should aid in the continued development of FTIs as therapeutics for the treatment of cancer and parasitic infections.

Although advances in medical science have greatly reduced the toll of many human diseases, cancer still presents challenges to effective treatment (*1*). The search for new cancer treatment targets has identified many signal transduction proteins involved in cell growth and differentiation that can contribute to oncogenesis upon mutation (*2*). All GTP-binding proteins (G proteins) known to be involved in oncogenesis, including members of the Rho and Ras superfamily, are modified by the essential post-translational attachment of an isoprenoid lipid (prenylation) near the C-terminus (*3*). Protein prenylation is absolutely required for the function of these proteins. Inhibition of protein prenylation provides an indirect means of downregulating errant cell growth signal transduction pathways. Protein prenyltransferase inhibitors represent a new class of cancer therapeutic (*4*), and these inhibitors have been evaluated in a number of phase I, II, and III clinical trials (*5*, *6*). Furthermore, preclinical evaluation indicates that protein prenyltransferase inhibitors could be used in the treatment of parasitic infections such as malaria (*7*), hepatitis C (*8*), and multiple sclerosis (*9*).

Protein prenylation is catalyzed by the two CaaX prenyltransferase family members, protein farnesyltransferase (FTase)[1] and protein geranylgeranyltransferase type I (GGTase-I), and Rab GGTase, which plays a more specialized role in the cell (*3*). FTase and GGTase-I catalyze the attachment of a 15-carbon farnesyl lipid from a farnesyl diphosphate donor (FPP, Figure 1a) and a 20-carbon geranylgeranyl lipid from a geranylgeranyl diphosphate donor (GGPP), respectively, to substrate proteins with a C-terminal Ca_1a_2X sequence motif (*10*, *11*). This motif consists of an invariant cysteine (C) to which the lipid is attached, two small aliphatic amino acids (a_1 and a_2), and a variable C-terminal amino acid (X) that determines whether the protein is a substrate for FTase, GGTase-I, or both (*10*, *11*). Farnesylation of oncogenic Ras proteins, which are associated with ∼30% of all human cancers (*2*), is essential for their transforming activity (*12*). Development of FTase inhibitors (FTIs) has progressed tremendously in the past 14 years, beginning with the initial discovery that some Ca_1a_2X tetrapeptides are inhibitory (*13*) and evolving into the development of Ca_1a_2X peptidomimetics and non-peptide-based inhibitors (*3*−*5*). Protein prenyltransferase inhibitors must be very specific toward one prenylation enzyme, because preclinical studies indicate that inhibition of both FTase and GGTase-I may be toxic (*14*). Crystal structures defining the reaction pathway of FTase and GGTase-I have been determined (*15*−*20*), as have structures of FTase complexed with inhibitors (*21*−*23*). Structures of FTase and GGTase-I indicate that the enzymes have similar active sites (*15*, *20*). Development of protein prenyltransferase inhibitors therefore greatly benefits from a detailed understanding of the molecular mechanisms that determine protein prenyltransferase inhibitor specificity.

The clinical candidates R115777 and BMS-214662 have been developed by the Janssen Research Foundation and Bristol-Myers Squibb, respectively (*6*, *24*). R115777 is a nonpeptide quinolone analogue FTI (*25*), and BMS-214662 is a nonpeptide tetrahydrobenzodiazepine FTI (Figure 1; ring

† This work was supported by a NIH Grant GM5238 to L.S.B.

* To whom correspondence should be addressed: Department of Biochemistry, Box 3711, Duke University Medical Center, Durham, NC 27710. Telephone: (919) 681-5267. Fax: (919) 684-8885. E-mail: lsb@biochem.duke.edu.

[1] Abbreviations: FTase, protein farnesyltransferase; FPP, farnesyl diphosphate; FTI, FTase inhibitor; GGTase-I, protein geranylgeranyltransferase type I; GGPP, geranylgeranyl diphosphate; SAR, structure−activity relationship.

10.1021/bi049723b CCC: $27.50
Published on Web 05/11/2004

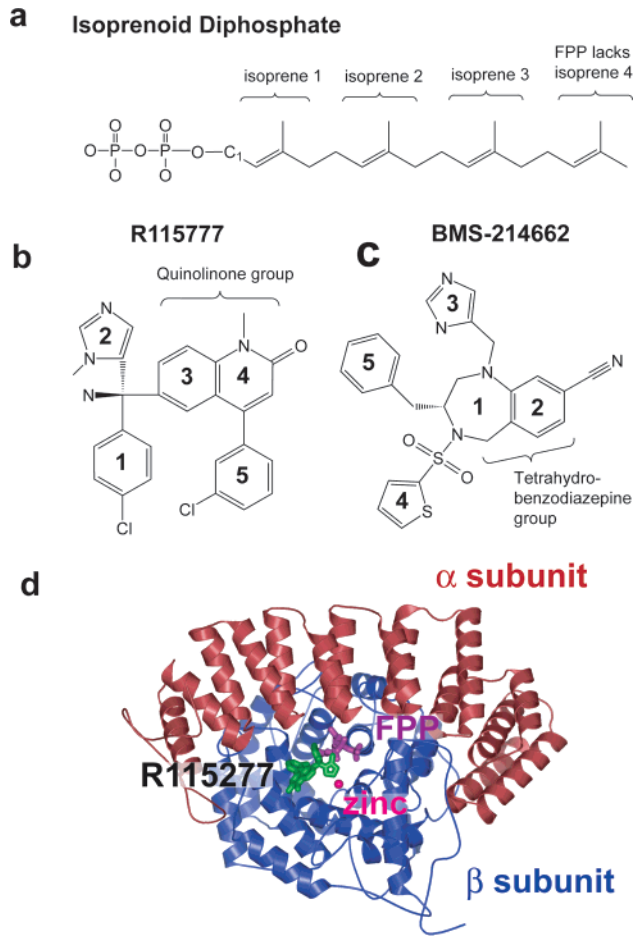

FIGURE 1: Chemical structures. (a) Farnesyl diphosphate (FPP) has three isoprene units; geranylgeranyl diphosphate (GGPP) has four. (b) Structure of R115777. (c) Structure of BMS-214662. (d) Ribbons cartoon of the FTase·FPP·R115777 structure in which the inhibitor is in green and the FPP lipid substrate in purple.

groups have been labeled 1−5 for clarity (*26*). Both drugs are selective toward FTase, and show almost no activity against GGTase-I. R115777 and BMS-214662 have been evaluated in a number of phase I and II clinical trials (*5*, *6*). R115777, the first FTI to advance to phase III clinical trials, shows indications for the treatment of blood and breast cancers (*27*, *28*). Here we present the first structural information for R115777 and BMS-214662 bound to FTase.

EXPERIMENTAL PROCEDURES

Sample Preparation and Crystallization. Human and rat FTase (hFTase and rFTase, respectively) were expressed, purified, and stored as previously described (*15*, *22*, *29*). Rat FTase crystallizes under a broader range of conditions and ligands than human FTase, and ligands can be soaked into the rFTase crystals without compromising diffraction quality (*19*, *21*, *22*). The sequences of rat and human FTase are 95% identical with complete sequence and structural conservation around the active site (backbone root-mean-square deviation of 0.4 Å) (*22*). The only differences between rat and human FTase structures occur at interprotein contact points in the crystal lattice, which is consistent with the differences in crystallization properties of these two enzymes. This structural and sequence conservation indicates that either enzyme serves well in the development and optimization of FTI's (*22*).

BMS-214662 and R115777 were prepared as previously described in the literature and were shown to be pure by HPLC and have the correct structures by NMR and electrospray ionization mass spectrometry (*24*, *30*). These compounds were prepared by Laxman Nallan and Pravine Bendale in Prof. M. H. Gelb's laboratory (University of Washington, Seattle, WA).

The hFTase·FPP·R115777 ternary complex was formed by incubating hFTase (15 mg/mL frozen stock solution) first with FPP [10 mM stock in 20 mM Tris-HCl (pH 7.7) from Sigma] on ice for 2 h, followed by incubation with R115777 (20 mM stock in DMSO) on ice for 3 h for a final hFTase:FPP:R115777 molar ratio of 1:3:1.5. The complex was crystallized, cryoprotected, and flash-cooled in liquid nitrogen as previously described (*22*). Although hFTase crystallized in the presence of BMS-214662, these crystals diffracted poorly. The rFTase·FPP·BMS-214622 ternary complex was formed by soaking a cocrystal of rFTase containing the farnesylated KKKSKTKCVIM product (*19*) in a stabilization solution supplemented with saturated BMS-2146222 (20 mM stock in DMSO) and 100 μM FPP for 1 week (*22*). Crystals were cryoprotected and flash-cooled in liquid nitrogen as previously described (*18*). Ligand binding in rFTase and hFTase has been previously demonstrated to be independent of the means by which the ligand is introduced (i.e., cocrystallization vs soaking) (*21*, *22*).

Data Collection, Model Building, and Refinement. Crystals were kept at 100 K during data collection (*31*). Diffraction data were measured at Advanced Photon Source station 14-BMC [Argonne National Laboratories (ANL-APS), Argonne, IL] and at National Synchrotron Light Source station X25 [Brookhaven National Laboratories (BNL-NSLS), Upton, NY]. DENZO and SCALEPACK were used for data reduction and scaling (*32*). Phases were determined using molecular replacement as implemented in CNS version 1.0 (*33*) using previously determined rFTase (PDB entry 1D8D) and hFTase (PDB entry 1JCQ) structures as a probe. Structure refinement consisted of iterative rounds of manual model building in O (*34*) followed by simulated annealing, minimization, and *B*-factor refinement (*33*). All included waters had at least a 3σ peak in omit $F_o - F_c$ maps, with density recapitulated in $2F_o - F_c$ maps. All active site ligands have continuous, well-defined omit density and are bound at full occupancy. REDUCE and PROBE were used to check for and eliminate clashes in the final structures (*35*). Table 1 contains a summary of diffraction data and refinement statistics. Sequence-based superpositions were created using Swiss PDB Viewer (*36*), and figures were made using PYMOL (*37*). Solvent-accessible surface areas were calculated using CNS version 1.0, employing a probe radius of 1.4 Å.

RESULTS

R115777 and BMS-214662 bind in the FTase active site, a deep hydrophobic cleft formed at the interface of the α- and β-subunits (Figure 1d). Drug binding does not induce a change in the structure of the active site, consistent with previous structures containing bound substrates, products, or inhibitors (*16*−*19*, *21*−*23*). All of the residues in contact with R115777 and BMS-214662 adopt the same conformation. Both drugs bind as a ternary complex with FPP and

Table 1: Data Collection and Refinement Statistics[a]

	hFTase·FPP·R115777	rFTase·FPP·BMS-214662
beamline	ANL-APS 14BMC	BNL-NSLS X25
wavelength (Å)	0.900	1.100
resolution (Å)	40−2.1 (2.18−2.10)	50−2.6 (2.69−2.60)
no. of unique/total reflections	66907/226817	35102/225013
mean I/σ_I	10.6 (3.0)	11.8 (3.7)
completeness (%)	96.6 (92.0)	98.7 (97.5)
R_{sym} (%)	8.7 (27.0)	11.0 (31.3)
cell dimensions $a = b$, c (Å)	178.2, 69.3	170.5, 69.0
R_{cryst} (%)	16.6 (23.0)	18.8 (29.5)
R_{free} (%)	19.5 (24.0)	22.5 (32.2)
no. of non-hydrogen atoms	6663	6291
no. of water molecules	672	280
Ramachandran plot, favored (%)	91.8	90.0
Ramachandran plot, allowed (%)	8.2	10.0
rmsd for bond lengths (Å)	0.006	0.007
rmsd for bond angles (deg)	1.2	1.2
average B-factor (Å^2)		
all	23.7	23.4
drug	16.9	17.1
σA coordinate error	0.22	0.44
PDB entry	1SA4	1SA5

[a] $R_{sym} = [\sum|(I - \langle I\rangle)|]/\sum I$, where $\langle I\rangle$ is the average intensity of multiple measurements. R_{cryst} and $R_{free} = (\sum|F_{obs} - F_{calc}|)/\sum|F_{obs}|$. R_{free} was calculated over 5% of the amplitudes not used in the refinement. Values in parentheses are for the outer resolution shell.

coordinate the catalytic zinc ion, which is located at the rim of the active site and bound at full occupancy.

FTase·FPP·R115777 Structure. R115777 binds to FTase in the substrate Ca_1a_2X peptide binding site, consistent with solution studies that indicate a peptide-competitive mechanism (Figure 2a) (*25*). For reference, a previously determined structure of a K-Ras substrate Ca_1a_2X peptide bound to FTase is shown in Figure 2c (*17*, *18*). FPP binds as observed in other complexes in an extended conformation (*16*, *19*, *21*−*23*), with one face of the isoprenoid moiety forming part of the R115777 binding surface. The drug adopts a U shape, stabilized by stacking between the *para*- and *meta*-substituted chlorophenyl rings (rings 1 and 5). The imidazole nitrogen (ring 2) juts out from the apex of the turn and coordinates the catalytic zinc at a nitrogen−zinc distance of 2.0 Å. In addition to zinc coordination, the drug forms water-mediated hydrogen bonds between the quinolinone carbonyl oxygen (ring 4) and the protein backbone (Phe 360β) and between the ring 1 amine group and the FPP α-phosphate moiety. Besides these polar interactions, R115777 forms only van der Waals contacts with the enzyme and the FPP farnesyl moiety. Aromatic stacking interactions (*38*) feature prominently among these contacts: ring 1 stacks against the farnesyl moiety of FPP, the quinolinone group (rings 3 and 4) stacks face on face with Tyr 361β, and the *meta*-substituted chlorophenyl group (ring 5) stacks edge on face with Trp 102β and Trp 106β. The position of ring 5 is consistent with previous structure−activity relationship (SAR) data that demonstrated strict size limitations for aromatic groups at this position as well as limitations on the positions of the chloride groups (*24*).

FTase·FPP·BMS-214662 Structure. BMS-214622 also binds to FTase in the Ca_1a_2X peptide binding site, consistent with solution studies that indicate a peptide-competitive mechanism (Figure 2b) (*30*). FPP binds as seen in the R115777 complex, and the third FPP isoprene unit forms part of the BMS-214622 binding surface. The central tetrahydrobenzodiazepine group (rings 1 and 2) adopts what appears to be a twisted boat conformation with the three substituent ring groups (rings 3−5) jutting out to interact with the protein and solvent. The imidazole group (ring 3) coordinates the catalytic zinc. Besides this polar interaction, BMS-214622 forms only van der Waals contacts with the protein and FPP farnesyl moiety. Rings 1 and 2 stack face on face with Tyr 361β, and the methylphenyl group (ring 5) is bound in a hydrophobic pocket, stabilized by stacking against the FPP farnesyl moiety and end-on-face stacking with Trp 102β and Trp 106β. This binding mode is consistent with prior SAR data that demonstrated strict size and polarity limitations for the ring 5 substituent (*26*). The thienylsulfonyl group (ring 4) is mostly solvent exposed, and stabilized primarily by stacking against rings 1 and 2. Previous SAR data demonstrated a high tolerance for different substituents at the ring 4 position without compromising inhibitory activity, consistent with the solvent accessibility of this group (*26*).

An interesting crystallographic artifact arose in the course of determining the FTase·FPP·BMS-214662 structure. The nitrogen−sulfur bond that links the BMS-214662 thienylsulfonyl group (ring 4) to the central tetrahydorbenzodiazepine group can be cleaved by ionizing radiation, even at cryogenic temperatures (100 K). Exposure to high-flux synchrotron X-rays ($\lambda = 1.00$ Å) causes a time-dependent decay of the electron density corresponding to ring 4. This decay was not observed when lower-flux X-rays ($\lambda = 1.54$ Å), generated by a rotating copper anode, were utilized (result

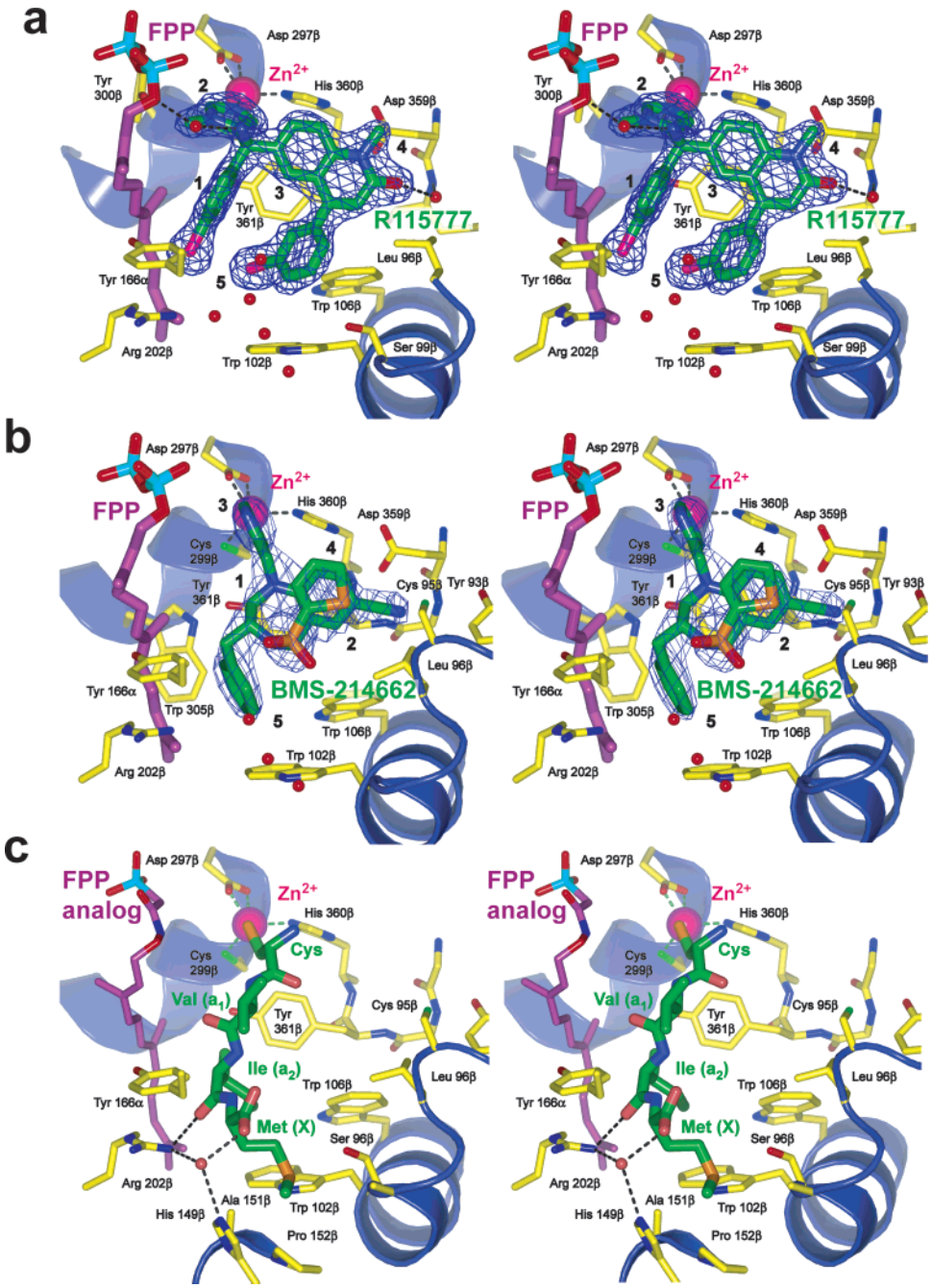

FIGURE 2: Inhibitors bound in the FTase active site. Electron density is shown at a $+5\sigma$ level and was calculated using $(F_{obs} - F_{calc})\alpha_{calc}$ Fourier coefficients with the inhibitor omitted from the final model. (a) Stereoview of the FTase·FPP·R115777 complex. R115777 (green) adopts a U shape, stabilized by stacking between the two chlorophenyl rings. The imidazole group coordinates the catalytic zinc (magenta). The drug makes extensive van der Waals contacts with the farnesyl moiety of FPP (purple) and with the protein. Two water-mediated hydrogen bonds are made to FPP and the protein. Five water molecules occupy the space where the X residue of the Ca_1a_2X peptide usually binds, the specificity pocket. (b) Stereoview of the FTase·FPP·BMS-214662 complex, shown in approximately the same orientation as panel a. The drug (green) coordinates the catalytic zinc and makes van der Waals contacts with the surrounding protein and FPP ligand. The drug does not contact the specificity pocket, which is occupied by three solvent molecules. (c) Stereoview of FTase complexed with a K-Ras substrate peptide KKKSKTKCVIM (only the Ca_1a_2X motif is shown, colored green) and a nonhydrolyzable FPP analogue (purple), shown in approximately the same orientation as panel A (PDB entry 1D8D) (*18*).

not shown). Loss of this drug moiety alters neither the conformation of the remainder of the drug nor the active site, relative to the complete BMS-214662 structure. This phenomenon necessitated rapid data collection at the synchrotron X-ray source, limiting usable diffraction to a resolution of 2.6 Å. Longer exposure times permitted collection of 2.1 Å diffraction data, and the overall structure of the protein and the drug (without ring 4) is essentially identical to the 2.6 Å structure when refined against the 2.1 Å data. The cleavage of disulfide linkages in protein crystals by high-flux X-rays is well-documented (*39*), but to our knowledge, this is the first example of radiation-induced ligand cleavage.

DISCUSSION

Comparison to Substrates and Products. Comparison of the BMS-214662 and R115777 complexes to structures of FTase complexed with various substrates and products

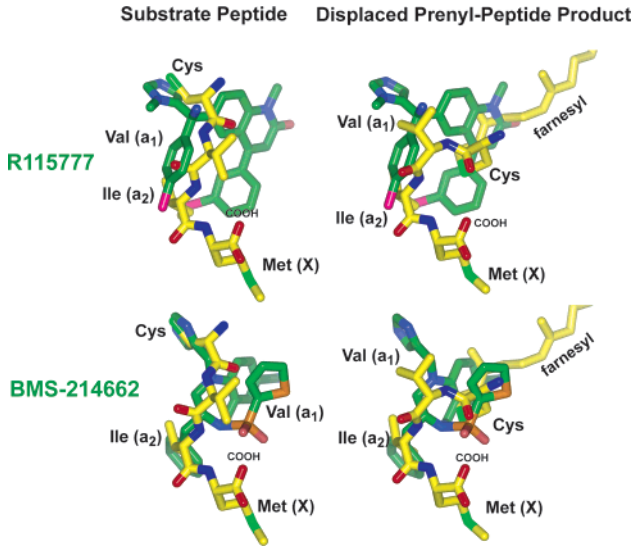

FIGURE 3: Comparison of FTase inhibitor complexes to FTase substrate and product complexes. Superpositions of the R115777 (top row) and BMS-214662 (bottom row) FTase complexes with FTase complexed with a K-Ras substrate peptide and FPP analogue (left column, PDB entry 1D8D) (*18*) or with FTase complexed with FPP and a farnesyled K-Ras peptide product (right column, PDB entry 1KZO) (*19*). The farnesyl−peptide product adopts two conformations as part of the FTase reaction cycle (*19*). The one shown here, the "displaced" conformation, occurs after binding of FPP displaces the farnesyl moiety of the product from the isoprenoid substrate binding site (see the text) (*19*). For clarity, only inhibitors, the Ca_1a_2X moiety of the substrate peptide, and the farnesylated Ca_1a_2X moiety of the product are shown. R115777 and BMS-214662 both overlap with the binding of the Ca_1a_2 portion of the Ca_1a_2X peptide bound in the extended substrate conformation. Additionally, both inhibitors overlap with the peptide and lipid moieties of the prenyl−peptide product bound in the displaced conformation.

reveals that these two drugs mimic different states from the FTase reaction coordinate. High-resolution complexes have allowed the structural biochemistry of the FTase reaction pathway to be defined (*15*−*19*). FPP binds first, followed by the substrate Ca_1a_2X peptide substrate. The Ca_1a_2X motif binds in an extended conformation, with the cysteine thiolate anchored to the zinc ion and the carboxyl terminus anchored ~12 Å away by hydrogen bonds (Figure 2c). After catalysis, the peptide−prenyl product is retained by the enzyme (*40*). FPP binding results in a translocation of the prenyl−peptide product; the Ca_1a_2X peptide adopts a type I β-turn, and the product farnesyl group is displaced (to make room for the incoming FPP) into a shallow solvent-accessible groove that extends from the active site to the rim of the β-subunit, the "exit groove". A comparison of the two inhibitors with the FTase peptide substrate K-Ras (CVIM Ca_1a_2X motif) illustrates that drug binding overlaps with the Ca_1a_2 portion of the Ca_1a_2X motif in both the "extended" binding mode and the displaced, type-I β-turn conformation (Figure 3). Furthermore, both drugs partially occupy the exit groove, overlapping with the displaced product farnesyl moiety. Traditionally, FTI design has focused on mimicking the substrate Ca_1a_2X peptide (*3*, *5*, *41*). These results, however, demonstrate that several peptide binding modes can be considered in the design of Ca_1a_2X-competitive FTIs.

Comparison of the R115777 and BMS-214662 structures to those from the FTase reaction coordinate reveals two inhibitor features that could be targeted to modulate inhibitor activity. First, both inhibitors are only ~60% buried by the protein and the adjacent FPP molecule. This may permit the addition of functional groups for modulation of bioavailability, toxicity, and stability without affecting drug binding or specificity. Second, R115777 and BMS-214662 form no direct hydrogen bonds with FTase, and structure-based design to take advantage of unsatisfied hydrogen bond donors or acceptors in the active site may be a means of modulating inhibitor affinity.

Comparison to Other FTIs. A comparison of R115777 and BMS-214662 complexes to other FTIs, including the anticancer clinical candidates SCH66336 (Lonafarnib/Sarasar), the peptidomimetic L739−750, the 3-aminopyrrolidinone FTI U49, and Abbott Laboratories biphenyl FTI, reveals two common features shared among peptide-competitive FTIs (*21*−*23*, *42*). First, all bind as a ternary complex with FPP and make extensive van der Waals contacts with the FPP lipid moiety (*17*, *18*). This is analogous to substrate peptide binding. Like these FTIs, FPP and the substrate Ca_1a_2X peptide form extensive van der Waals contacts. These contacts necessitate ordered substrate binding, with FPP binding first, and Ca_1a_2X peptide binding in the absence of FPP is low-affinity and transient (*43*). A similar phenomenon has been observed with SCH66336, which requires FPP to form a high-affinity complex with FTase (*21*). This suggests that, like substrate binding, FTI binding is ordered, and that FPP must be first bound to FTase to form the high-affinity FTase·FTI complex. Second, this comparison illustrates that these six FTIs have aromatic rings positioned where the a_2 residue of substrate Ca_1a_2X peptides binds. The "a_2 binding site" consists of residues Trp 102β, Trp 106β, Tyr 361β, and the third FPP farnesyl moiety, and all of these inhibitors form face-on-face or edge-on-face aromatic stacking interactions with one or more of these residues. Aromatic stacking interactions can contribute significantly to ligand binding energy (*38*, *44*), and aromatic rings that form interactions with the FTase a_2 binding site appear to be an important component of FTI chemistry. This shared feature of aromatic stacking interactions among these six FTIs is surprising, given their development through independent drug discovery mechanisms. An analogous example of "convergent evolution" in the natural world is found in peptide K^+ channel inhibitors from different animal species; these small peptide toxins possess different folds, but the topology of key residues is identical (*45*).

A Molecular Model of Inhibitor Selectivity. R115777 and BMS-214662 are very specific FTase inhibitors, both exhibiting a >1000-fold preference over GGTase-I (*25*, *26*). Surprisingly, neither inhibitor achieves this selectivity through interactions with the FTase residues that discriminate between FTase and GGTase-I Ca_1a_2X peptide substrates. FTase and GGTase-I have unique "specificity pockets", which select cognate peptide substrates through steric complementarity with the Ca_1a_2X motif X residue, which is generally Met, Gln, or Ser for FTase substrates and Leu for GGTase-I substrates (*10*, *11*, *17*, *18*, *20*). Neither drug occupies the specificity pocket (Figures 2a,b). A superposition of the two FTase structures and GGTase-I illustrates how R115777 and BMS-214662 achieve selectivity toward FTase without using the FTase selectivity pocket. The superposition reveals that in GGTase-I there are no residues that would interfere sterically or electrostatically with R115777 or BMS-214662.

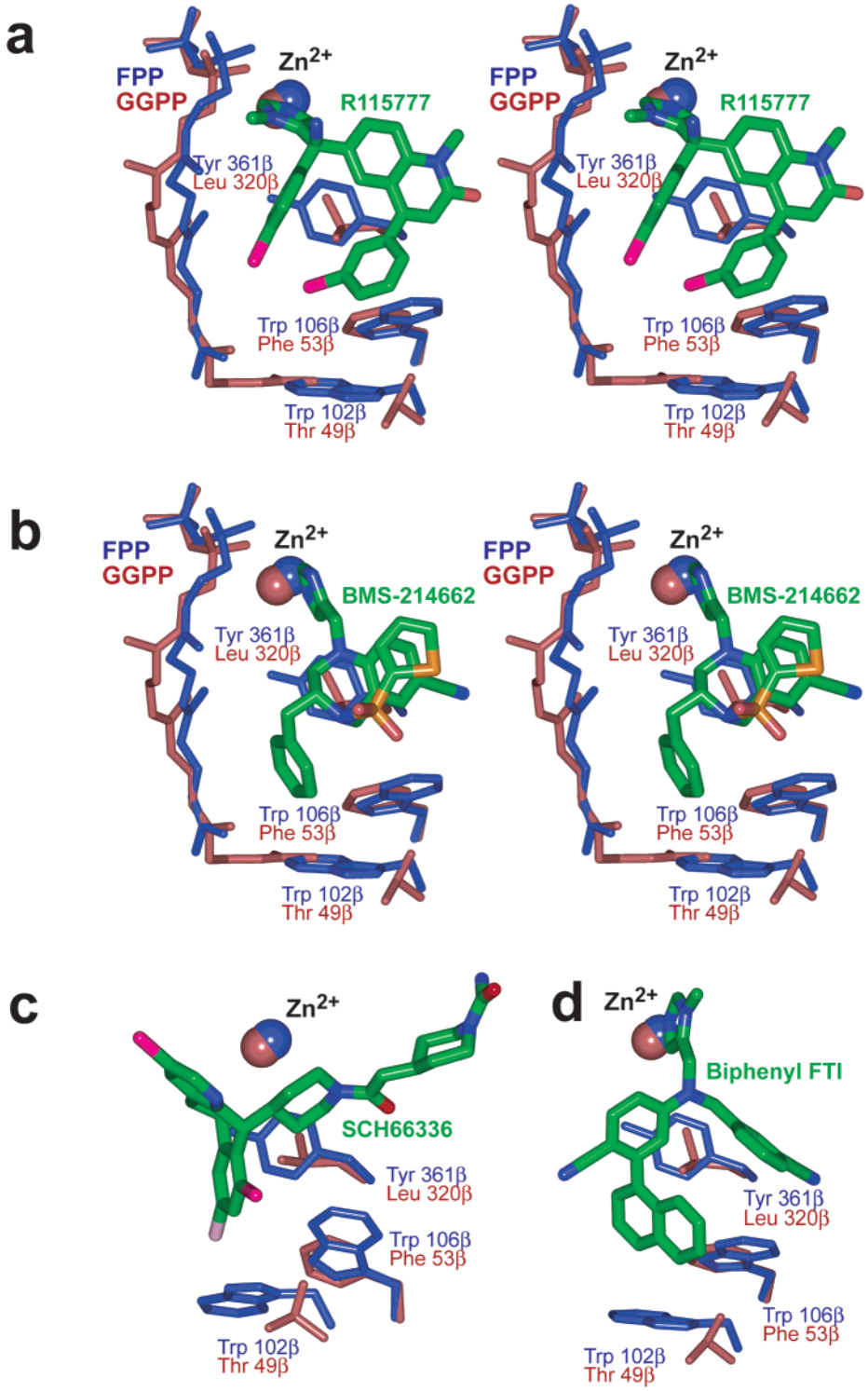

FIGURE 4: Superposition of FTase and GGTase-I suggests a molecular mechanism for inhibitor selectivity. Stereopair showing a superposition of a GGTase-I−GGPP complex (red) (PDB entry 1N4P) (*20*) with FTase complexes R115777 (a) and BMS-214662 complexes (b) (blue). A cluster of three aromatic residues, the a_2 binding site, form face-on-face and edge-on-face stacking interactions with R115777 and BMS-214662 in the FTase active site. The residues that constitute the equivalent GGTase-I a_2 binding site does not permit the same stacking interactions, suggesting that aromatic stacking interactions determine inhibitor selectivity toward FTase. Superposition of FTase (blue) complexed with the inhibitors SCH66336 (c) (PDB entry 1O5M, green) (*21*) or the Abbott Laboratories biphenyl FTI (d) (PDB entry 1NL4, green) (*42*) with a GGTase-I−GGPP complex (red) suggests that these two inhibitors achieve selectivity toward FTase through a similar mechanism.

Instead, the only substantial differences are in the GGTase-I a_2 binding site, which consists of residues Thr 49β, Phe 53β, and Leu 320β, contrasted to Trp 102β, Trp 106β, and Tyr 361β in FTase, respectively (Figure 4a,b). These differences eliminate all potential direct and end-on stacking interactions with either inhibitor, suggesting that R115777 and BSM-214662 achieve selectivity toward FTase through selective aromatic stacking interactions with the a_2 binding site. Analysis of available FTase·FTI structures reveals that other FTIs may also selectively inhibit FTase through this mechanism. Examples include the clinical candidate SCH66336 and Abbott Laboratories biphenyl FTI, which show 10000-

and 400-fold selectivity toward FTase over GGTase-I, respectively (*42*, *46*). Like R115777 and BMS-214662, these two inhibitors do not explicitly occupy the specificity pocket and form extensive stacking interactions with the FTase a_2 binding site, whereas in GGTase-I, these stacking interactions are not possible (Figure 4c,d) (*21*, *42*). In agreement with this hypothesis, mutations that alter the aromatic and steric character of the a_2 binding site to resemble that of GGTase-I renders FTase resistant to FTIs such as SCH66336 (*47*). These results illustrate the fact that aromatic groups that complement the a_2 binding site are an important feature of FTIs, and indicate specificity toward FTase can be achieved by matching the unique steric and aromatic properties of the a_2 binding site alone.

R115777, BMS-214662, and other FTIs show promise for the treatment of parasitic infections such as *Plasmodium falciparum* (malaria), *Trypanosoma* (sleeping sickness and Chagas disease), and *Entamoeba histolytica* (amoebic dysentery) (*48*, *49*). Sequence alignments indicate that the residues that constitute the a_2 binding site are conserved in these protists, suggesting that R115777 and BMS-214662 will bind in parasite FTase orthologs like they do in mammalian FTase (*48*, *50*, *51*). FTase from parasites has peptide substrate selectivity slightly different from that of mammalian FTase, and sequence alignments reveal that the residues that constitute the specificity pocket in these enzymes are significantly different than in mammalian FTase (*48*, *50*, *51*). The addition of substituents to R115777 and BMS-214662 that exploit these differences may be a means of creating parasite-selective FTase inhibitors.

CONCLUSIONS

The two structures presented in this study suggest the molecular basis of FTase inhibition by R115777 and BMS-214662 and, when contrasted with the structure of GGTase-I, illustrate the mechanism of drug selectivity. This comparison also illustrates unique features of the FTase active site, most notably the aromatic residues constituting the Ca_1a_2X motif a_2 binding site, that can be targeted for selective inhibition and provides a framework for understanding FTI specificity. Finally, these structures should allow calibration of available SAR data, facilitate optimization of lead compounds, and perhaps aid in the design of new classes of protein prenyltransferase inhibitors.

ACKNOWLEDGMENT

We thank Mike Gelb for the kind gift of R115777 and BMS-214622, Bob Immormino and Kim Terry for assistance with FTase crystallization, and the ANL-APS BioCARS, ANL-APS SER-CAT, and BNL-NSLS X25 staff for their assistance. Research carried out (in whole or in part) at NSLS is supported by the U.S. Department of Energy, Division of Materials Sciences and Division of Chemical Sciences, under Contract DE-AC02-98CH10886. Use of the APS was supported by the U.S. Department of Energy, Basic Energy Sciences, Office of Science, under Contract W-31-109-Eng-38. Use of BioCARS Sector 14 was supported by the National Institutes of Health (NIH), National Center for Research Resources, under Grant RR07707.

REFERENCES

1. Stewart, B. W., and Kleihues, P. (2003) *World Cancer Report*, pp 352, World Health Organization International Agency for Research on Cancer, Lyon, France.
2. Barbacid, M. (1987) ras Genes, *Annu. Rev. Biochem. 56*, 779−827.
3. Tamanoi, F., and Sigman, D. S. (2001) Protein Lipidation, in *The Enzymes*, pp 322, Academic Press, San Diego.
4. Sebti, S. M., and Hamilton, A. D. (2000) Farnesyltransferase and geranylgeranyltransferase I inhibitors and cancer therapy: lessons from mechanism and bench-to-bedside translational studies, *Oncogene 19*, 6584−6593.
5. Dinsmore, C. J., and Bell, I. M. (2003) Inhibitors of farnesyltransferase and geranylgeranyltransferase-I for antitumor therapy: substrate-based design, conformational constraint and biological activity, *Curr. Top. Med. Chem. 3*, 1075−1093.
6. Caponigro, F., Casale, M., and Bryce, J. (2003) Farnesyl transferase inhibitors in clinical development, *Expert Opin. Invest. Drugs 12*, 943−954.
7. Chakrabarti, D., Azam, T., DelVecchio, C., Qiu, L., Park, Y. I., *et al*. (1998) Protein prenyl transferase activities of *Plasmodium falciparum*, *Mol. Biochem. Parasitol. 94*, 175−184.
8. Ye, J., Wang, C., Sumpter, R., Jr., Brown, M. S., Goldstein, J. L., *et al.* (2003) Disruption of hepatitis C virus RNA replication through inhibition of host protein geranylgeranylation, *Proc. Natl. Acad. Sci. U.S.A. 100*, 15865−15870.
9. Walters, C. E., Pryce, G., Hankey, D. J., Sebti, S. M., Hamilton, A. D., *et al.* (2002) Inhibition of Rho GTPases with protein prenyltransferase inhibitors prevents leukocyte recruitment to the central nervous system and attenuates clinical signs of disease in an animal model of multiple sclerosis, *J. Immunol. 168*, 4087−4094.
10. Yokoyama, K., Goodwin, G. W., Ghomashchi, F., Glomset, J. A., and Gelb, M. H. (1991) A protein geranylgeranyltransferase from bovine brain: Implications for protein prenylation specificity, *Proc. Natl. Acad. Sci. U.S.A. 88*, 5302−5306.
11. Fu, H. W., and Casey, P. J. (1999) Enzymology and biology of CaaX protein prenylation, *Recent Prog. Horm. Res. 54*, 315−342.
12. Kato, K., Cox, A. D., Hisaka, M. M., Graham, S. M., Buss, J. E., *et al.* (1992) Isoprenoid addition to Ras protein is the critical modification for its membrane association and transforming activity, *Proc. Natl. Acad. Sci. U.S.A. 89*, 6403−6407.
13. Reiss, Y., Goldstein, J. L., Seabra, M. C., Casey, P. J., and Brown, M. S. (1990) Inhibition of purified p21ras farnesyl:protein transferase by Cys-AAX tetrapeptides, *Cell 62*, 81−88.
14. deSolms, S. J., Ciccarone, T. M., MacTough, S. C., Shaw, A. W., Buser, C. A., *et al.* (2003) Dual protein farnesyltransferase: geranylgeranyltransferase-I inhibitors as potential cancer chemotherapeutic agents, *J. Med. Chem. 46*, 2973−2984.
15. Park, H.-W., Boduluri, S. R., Moomaw, J. F., Casey, P. J., and Beese, L. S. (1997) Crystal structure of protein farnesyltransferase at 2.25 Å resolution, *Science 275*, 1800−1804.
16. Long, S. B., Casey, P. J., and Beese, L. S. (1998) Co-Crystal Structure of Protein Farnesyltransferase with a Farnesyl Diphosphate Substrate, *Biochemistry 37*, 9612−9618.
17. Strickland, C. L., Windsor, W. T., Syto, R., Wang, L., Bond, R., *et al.* (1998) Crystal Structure of Farnesyl Protein Transferase Complexed with a CaaX Peptide and Farnesyl Diphosphate Analogue, *Biochemistry 37*, 16601−16611.
18. Long, S. B., Casey, P. J., and Beese, L. S. (2000) The basis for K-Ras4B binding specificity to protein farnesyltransferase revealed by 2 Å resolution ternary complex structures, *Structure 8*, 209−222.
19. Long, S. B., Casey, P. J., and Beese, L. S. (2002) Reaction path of protein farnesyltransferase at atomic resolution, *Nature 419*, 645−650.
20. Taylor, J. S., Reid, T. S., Terry, K. L., Casey, P. J., and Beese, L. S. (2003) Structure of mammalian protein geranylgeranyltransferase type-I, *EMBO J. 22*, 5963−5974.
21. Strickland, C. L., Weber, P. C., Windsor, W. T., Wu, Z., Le, H. V., *et al.* (1999) Tricyclic farnesyl protein transferase inhibitors: crystallographic and calorimetric studies of structure−activity relationships, *J. Med. Chem. 42*, 2125−2135.
22. Long, S. B., Hancock, P. J., Kral, A. M., Hellinga, H. W., and Beese, L. S. (2001) The crystal structure of human protein farnesyltransferase reveals the basis for inhibition by CaaX tetrapeptides and their mimetics, *Proc. Natl. Acad. Sci. U.S.A. 98*, 12948−12953.
23. Bell, I. M., Gallicchio, S. N., Abrams, M., Beese, L. S., Beshore, D. C., *et al.* (2002) 3-Aminopyrrolidinone farnesyltransferase

inhibitors: design of macrocyclic compounds with improved pharmacokinetics and excellent cell potency, *J. Med. Chem. 45*, 2388−2409.
24. Venet, M., End, D., and Angibaud, P. (2003) Farnesyl protein transferase inhibitor ZARNESTRA R115777: history of a discovery, *Curr. Top. Med. Chem. 3*, 1095−1102.
25. End, D. W., Smets, G., Todd, A. V., Applegate, T. L., Fuery, C. J., *et al.* (2001) Characterization of the antitumor effects of the selective farnesyl protein transferase inhibitor R115777 in vivo and in vitro, *Cancer Res. 61*, 131−137.
26. Hunt, J. T., Ding, C. Z., Batorsky, R., Bednarz, M., Bhide, R., *et al.* (2000) Discovery of (*R*)-7-cyano-2,3,4,5-tetrahydro-1-(1*H*-imidazol-4-ylmethyl)-3-(phenylmethyl)-4-(2-thienylsulfonyl)-1*H*-1,4-benzodiazepine (BMS-214662), a farnesyltransferase inhibitor with potent preclinical antitumor activity, *J. Med. Chem. 43*, 3587−3595.
27. Kelland, L. R. (2003) Farnesyl transferase inhibitors in the treatment of breast cancer, *Expert Opin. Invest. Drugs 12*, 413−421.
28. Morgan, M. A., Ganser, A., and Reuter, C. W. (2003) Therapeutic efficacy of prenylation inhibitors in the treatment of myeloid leukemia, *Leukemia 17*, 1482−1498.
29. Chen, W.-J., Moomaw, J. F., Overton, L., Kost, T. A., and Casey, P. J. (1993) High-level expression of mammalian protein farnesyltransferase in a baculovirus system: the purified protein contains zinc, *J. Biol. Chem. 268*, 9675−9680.
30. Ding, C. Z., Batorsky, R., Bhide, R., Chao, H. J., Cho, Y., *et al.* (1999) Discovery and structure−activity relationships of imidazole-containing tetrahydrobenzodiazepine inhibitors of farnesyltransferase, *J. Med. Chem. 42*, 5241−5253.
31. Garman, E. (1999) Cool data: quantity AND quality, *Acta Crystallogr. D55*, 1641−1653.
32. Otwinowski, Z. and Minor, W. (1997) *Methods in Enzymology, Macromolecular Crystallography* (*Part A*): *Processing of X-ray Diffraction Data Collected in Oscillation Mode*, Vol. 20, 276 ed., Academic Press, New York, New York.
33. Brünger, A. T., Adams, P. D., Clore, G. M., DeLano, W. L., Gros, P., *et al.* (1998) Crystallography & NMR System: A New Software Suite for Marcomolecular Structure Determination, *Acta Crystallogr. D54*, 905−921.
34. Jones, T. A., Zou, J. Y., Cowan, S. W., and Kjeldgaard, M. (1991) Improved methods for binding protein models in electron density maps and the location of errors in these models, *Acta Crystallogr. A47*, 110−119.
35. Word, J. M., Lovell, S. C., LaBean, T. H., Taylor, H. C., Zalis, M. E., *et al.* (1999) Visualizing and quantifying molecular goodness-of-fit: small-probe contact dots with explicit hydrogen atoms, *J. Mol. Biol. 285*, 1711−1733.
36. Guex, N., and Peitsch, M. C. (1997) SWISS-MODEL and the Swiss-PdbViewer: an environment for comparative protein modeling, *Electrophoresis 18*, 2714−2723.
37. Delano, W. L. (2002) *PyMOL*, DeLano Scientific, San Carlos, CA.
38. Tatko, C. D. (2002) *Aromatic Interactions in Biological Systems*, pp 4, American Chemical Society, Washington, DC.
39. Weik, M., Ravelli, R. B., Kryger, G., McSweeney, S., Raves, M. L., *et al.* (2000) Specific chemical and structural damage to proteins produced by synchrotron radiation, *Proc. Natl. Acad. Sci. U.S.A. 97*, 623−628.
40. Tschantz, W. R., Furfine, E. S., and Casey, P. J. (1997) Substrate binding is required for release of product from mammalian protein farnesyltransferase, *J. Biol. Chem. 272*, 9989−9993.
41. Sebti, S. M., and Hamilton, A. D. (2000) Farnesyltransferase and geranylgeranyltransferase I inhibitors in cancer therapy: important mechanistic and bench to bedside issues, *Expert Opin. Invest. Drugs 9*, 2767−2782.
42. Curtin, M. L., Florjancic, A. S., Cohen, J., Gu, W.-Z., Frost, D. J., *et al.* (2003) Novel and Selective Imidazole-Containing Biphenyl Inhibitors of Protein Farnesyltransferase, *Bioorg. Med. Chem. Lett. 13*, 1367−1371.
43. Pompliano, D. L., Schaber, M. D., Mosser, S. D., Omer, C. A., Shafer, J. A., *et al.* (1993) Isoprenoid diphosphate utilization by recombinant human farnesyl:protein transferase: Interactive binding between substrates and a preferred kinetic pathway, *Biochemistry 32*, 8341−8347.
44. Jorgensen, W. L., and Severance, D. L. (1990) Aromatic−Aromatic Interactions: Free Energy Profiles for the Benzene Dimer in Water, Chloroform, and Liquid Benzene, *J. Am. Chem. Soc. 112*, 4768−4774.
45. Dauplais, M., Lecoq, A., Song, J., Cotton, J., Jamin, N., *et al.* (1997) On the convergent evolution of animal toxins. Conservation of a diad of functional residues in potassium channel-blocking toxins with unrelated structures, *J. Biol. Chem. 272*, 4302−4309.
46. Njoroge, F. G., Taveras, A. G., Kelly, J., Remiszewski, S., Mallams, A. K., *et al.* (1998) (+)-4-[2-[4-(8-Chloro-3,10-dibromo-6,11-dihydro-5*H*-benzo[5,6]-cyclohepta[1,2-*b*]pyridin-11(*R*)-yl-1-piperidinyl]-2-oxoethyl]-1-piperidinecarboxamide (SCH-66336): A very potent farnesyl protein transferase inhibitor as a novel antitumor agent, *J. Med. Chem. 41*, 4890−4902.
47. Del Villar, K., Urano, J., Guo, L., and Tamanoi, F. (1999) A mutant form of human protein farnesyltransferase exhibits increased resistance to farnesyltransferase inhibitors, *J. Biol. Chem. 274*, 27010−27017.
48. Kumagai, M., Makioka, A., Takeuchi, T., and Nozaki, T. (2004) Molecular Cloning and Characterization of a Protein Farnesyltransferase from the Enteric Protozoan Parasite *Entamoeba histolytica*, *J. Biol. Chem. 279*, 2316−2323.
49. Gelb, M. H., Van Voorhis, W. C., Buckner, F. S., Yokoyama, K., Eastman, R., *et al.* (2003) Protein farnesyl and N-myristoyl transferases: piggy-back medicinal chemistry targets for the development of antitrypanosomatid and antimalarial therapeutics, *Mol. Biochem. Parasitol. 126*, 155−163.
50. Yokoyama, K., Trobridge, P., Buckner, F. S., Van Voorhis, W. C., Stuart, K. D., *et al.* (1998) Protein farnesyltransferase from *Trypanosoma brucei*. A heterodimer of 61- and 65-kda subunits as a new target for antiparasite therapeutics, *J. Biol. Chem. 273*, 26497−26505.
51. Buckner, F. S., Eastman, R. T., Nepomuceno-Silva, J. L., Speelmon, E. C., Myler, P. J., *et al.* (2002) Cloning, heterologous expression, and substrate specificities of protein farnesyltransferases from *Trypanosoma cruzi* and Leishmania major, *Mol. Biochem. Parasitol. 122*, 181−188.

BI049723B